PCCP

Accepted Manuscript

ROYAL SOCIETY OF CHEMISTRY

www.rsc.org/pccp

Energy & Environmental Science

RSCPublishing

ARTICLE

Photoinduced water splitting with oxotitanium tetraphenylporphyrin

Cite this: DOI: 10.1039/x0xx00000x

O. Morawski, K. Izdebska, E. Karpiuk, J. Nowacki, A. Suchocki and A. L. Sobolewski*

Received 00th March 2014,
Accepted 00th March 2014

DOI: 10.1039/x0xx00000x

www.rsc.org/

Photocatalytic splitting of water was investigated in a heterogeneous system consisting of micro-crystallites of oxotitanium tetraphenylporphyrin deposited on fused silica plates, immersed in water and excited within the visible range of their absorption spectra. The water photolysis was evidenced by the spectroscopic detection of hydroxyl radicals generated in the reaction. The experimental results confirm the mechanism of water splitting and generation of $OH^{\bullet}$ radicals proposed theoretically by Sobolewski and Domcke [PCCP, 2012, 14, 12807] for the oxotitaniumporphyrin-water complex. It is shown that photocatalytic water splitting occurs in pure water, and neither pH-bias nor external voltage is required to promote the reaction.

Introduction

Water splitting with visible light is considered as one of the most challenging and important reactions for storing the energy of solar radiation in the form of chemical energy. The extensive research efforts towards solar water splitting are generally based on two alternative strategies: (i) the photoelectrochemical approach, first demonstrated by Fujishima and Honda [1], and (ii) the biomimetic approach, inspired by the current understanding of the processes in natural photosynthesis. In the former approach, electrons and holes generated by the absorption of light in a semiconductor are used to neutralize protons and hydroxide anions in an electrochemical cell. [2-7]. In the latter approach, supramolecular structures typically consisting of an organic chromophore, an electron donor, and an electron acceptor, have been constructed [8–14]. The absorption of a photon by the chromophore results in a charge-separation process which oxidizes the electron donor and reduces the electron acceptor. The oxidized donor and reduced acceptor moieties will eventually neutralize hydroxide anions and protons, respectively.

In an alternative approach to solar water splitting recently proposed by one of us (ALS), a strategy was explored which aims at the direct photoinduced homolytic cleavage of H_2O molecules into $H^{\bullet}$ and $OH^{\bullet}$ radicals by a photocatalytically active chromophore - oxotitanium porphyrin (TiPO) [15]. In this approach, the porphyrin moiety serves as the antenna for visible light absorption, while the TiO group exhibits the redox properties needed for the oxidation of water. Electronic-structure calculations performed in this work revealed that two singlet states of intramolecular charge-transfer (CT) character are located between the Q and B (Soret) absorption bands of the porphyrin ring. The wave functions of the CT states are single determinants, corresponding to the promotion of an electron from the HOMO or HOMO–1 π-orbitals of the porphyrin ring to a d-orbital of the central titanium atom. $Ti^{(IV)}$ in the electronic ground state and in the Q and B states is converted to $Ti^{(III)}$ in the CT states. These states are thus ligand-to-metal charge-transfer (LMCT) states. While the reactive LMCT states carry no oscillator strength, they can be populated by a radiationless transition from the strongly allowed Soret band of the porphyrin ring.

Extensive theoretical explorations of the photophysics of the hydrogen-bonded complex of TiPO with a single water molecule ($TiPO–H_2O$) performed in that work revealed a remarkable electronic charge rearrangement in the LMCT states which occurs through an electron-driven proton-transfer (EDPT) reaction in the excited state: the hole in the π-orbital of porphyrin is filled by electronic charge from the water molecule, upon which a proton follows, resulting in the formation of a hydrogen-bonded neutral $TiPOH^{\bullet}–OH^{\bullet}$ biradical. It was also shown that the water-splitting process in the $TiPO–H_2O$ complex can be completed by the absorption of a second photon by the $TiPOH^{\bullet}$ radical via its B band and radiationless population of a lower-lying dark $\pi\sigma^*$ doublet state which provides a channel for barrierless photodetachment of the $H^{\bullet}$ radical from $TiPOH^{\bullet}$. After the absorption of two visible photons, a water molecule is thus cleaved into free $OH^{\bullet}$ and $H^{\bullet}$ radicals and the photocatalyzer TiPO is recovered.

The present work aims at the experimental verification of the first stage of the water splitting reaction predicted in Ref. 15, that is, the formation of $OH^{\bullet}$ radicals due to absorption of a visible photon by the chromophore. The oxotitanium tetraphenylporphyrin (TiPPO) compound has been selected for our study as it is chemically more stable than the TiPO molecule, forms hydrogen bonded complexes with water like the former molecule does, and has similar photophysical

properties, as is shown by the accompanying electronic structure calculations.

Experimental

Oxotitanium tetraphenylporphyrin (TiPPO, Fig.1) was prepared with 95% yield by 24 h refluxing of a solution of *meso*-tetraphenylporphyrin (Alfa Aesar) and titanium tetrachloride in DMF containing 1% (vol.) of pyridine [16].

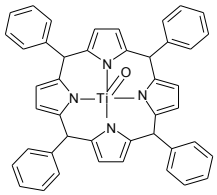

Figure 1. The structure of oxotitanium tetraphenylporphyrin molecule.

Since TiPPO does not dissolve in water, it was deposited for the photochemical experiments either on bare fused silica plates or on fused silica plates covered by a thin gold layer in order to attain electrical contact for current measurements. Deposition was performed in a vacuum evaporator type JEE 48 of Japan Electron Optics Laboratory Co. Ltd. under high vacuum condition (pressure of the order of 10^{-6} hPa). The evaporated molecular layer had a thickness of ca. 1 μm. The fused silica plates and gold electrode plates had a size of 45 x 8 x 1.5 mm. In most of these experiments, standard fused silica cuvettes of inner dimensions 4.5 x 1 x 1 cm were used; only for low-volume saturation measurements cuvettes of inner size 0.2 x 1 x 4.5 cm were used.

Absorption spectra have been measured with a Varian Cary 5000 UV-VIS-NIR absorption spectrometer. Fluorescence and fluorescence excitation spectra have been recorded with a Perkin-Elmer Model 512 fluorescence spectrometer. Photovoltaic measurements were performed in a quartz cuvette filled with neat deionized water and two immersed gold electrodes (one with deposited molecular layer). Two identical gold electrodes were used to avoid any bias arising from differences in (standard) electrode potentials. Photoresponse excitation spectra were recorded using one gold electrode (with deposited molecular layer) and a platinum wire separated by 4 mm as the second electrode. Voltage and current were measured on a Keithly Model 197 microvolt voltmeter. In all measurements, distilled and deionized water of conductivity 0.□□□S/cm was used. The selective irradiation of molecular layers of TiPPO was performed with a Mira laser pumped by a Verdi laser of Coherent Inc. and solid–state lasers of Ultralasers Inc..

For the detection of hydroxyl radicals we used a well-known OH scavenger, terephthalic acid (benzene-1,4-dicarboxylic acid) which does not react with other radicals potentially present in the sample such as O_2^-, HO_2 or H_2O_2 [17-19]. By the reaction with $OH^\bullet$ radicals, the non-fluorescent terephthalic acid (TA) is converted into hydroxyterephthalic acid (HTA), which shows strong fluorescence with a maximum at 425 nm when exited in the range of 310 – 315 nm. The solution of TA was prepared in pure, distilled and deionized water by dissolving first NaOH (35×10^{-4} M) and then TA (5×10^{-4} M). The TiPPO plates were immersed in this solution, irradiated for a given time at a wavelength corresponding to either the Q band or the Soret band and the fluorescence spectrum of the solution was recorded with excitation at 315 nm. In this way, we were able to detect the photo-production of hydroxyl radicals from water by measuring the increase of the HTA fluorescence after irradiation of the plates with deposited TiPPO molecules.

The indirect detection of hydroxyl radicals allows us to estimate only a lower limit of the efficiency of the water splitting reaction, since HTA is produced in a chain of reactions. The first of these is the actual splitting of water into biradicals

$$TiPPO + H_2O + h\nu \rightarrow TiPPOH^\bullet + OH^\bullet \quad (1)$$

The hydroxyl radicals diffuse to encounter terephthalic acid and react with the latter to give hydroxyterephthalic acid and water

$$TA + 2OH^\bullet \rightarrow HTA + H_2O \quad (2)$$

The simplifications in the above scheme are that the $OH^\bullet + OH^\bullet \rightarrow H_2O_2$ reaction and the possible reaction of $OH^\bullet$ with TiPPO are neglected. These reactions compete with (1) and (2). Therefore, the experimentally determined efficiency of TA → HTA conversion represents a lower limit for the water splitting efficiency.

The use of TA, which is insoluble in pure water, as $OH^\bullet$ scavenger requires a rather high concentration of NaOH to render TA soluble, which affects the pH of the solution. To be sure that the reaction (1) occurs also in pure water, we applied another $OH^\bullet$ scavenger - benzoic acid (BA) – which dissolves much better than TA in neat water and therefore does not require the addition of NaOH. BA is known to attach hydroxyl radicals at the ortho, meta, and para positions to form o-, m- and p-hydroxybenzoic acid with a nearly statistical distribution of isomers ($k_{ortho} : k_{meta} : k_{para}$) = 0.7 : 0.9 : 1) [27]. To detect the presence of $OH^\bullet$, we measured the fluorescence of 2-hydroxybenzoic acid (salicylic acid, SA) which absorbs at lower energies than BA [28].

Theoretical calculations for TiPPO-H_2O

The equilibrium geometry of the hydrogen-bonded complex of TiPPO with a single water molecule (TiPPO-H_2O) in the electronic ground state was determined with density functional theory (DFT), employing the B3LYP functional. The vertical excitation energies of the lowest excited singlet states were calculated with the time-dependent DFT (TD-DFT) method, employing the same functional. The equilibrium geometry of the photoproduct of the reaction, the biradical $TiPPOH^\bullet$-$OH^\bullet$, was obtained by geometry optimization of the lowest open-shell singlet (or triplet) state at the spin-unrestricted DFT (UDFT) level. The correlation-consistent double-zeta basis set (cc-pVDZ) was employed for the first-row atoms, while the cc-pVTZ basis was used for the Ti atom [20]. The TURBOMOLE program package was used for all electronic-structure calculations [21,22].

Extensive explorations of the spectroscopic and photophysical properties of TiPO and TiPO-H_2O, performed in Ref. 15 with several electronic-structure methods, have led to the conclusion that the TD-DFT/UDFT protocol is a reliable computational method for this kind of molecular systems.

Results

The Scanning Electron Microscope (SEM) image of TiPPO deposited on a fused silica plate is shown in Fig. 2a. It crystalizes in the form of micro-crystallites. The stability of the evaporated molecular layer was checked by comparison of the absorption spectra of (i) the plate with TiPPO in air, (ii) the plate immersed in a solution of TA in water and (iii) the plate in a solution of TA in water after exposition to 20 minutes irradiation at 445 nm with a 50 mW solid-state laser. No changes in the shape or absorbance of the Soret band (at 445 nm) and the Q band (at 555 nm) were noticed in these experiments for up to three hours of irradiation (Fig. 3). However, after 4.5 hours of irradiation we observed a 40% decrease of the optical density. This is accompanied by changes in the SEM image of the layer (Fig. 2b), where it is seen that the surface is considerably modified. When a plate with deposited TiPPO is immersed in neat deionized water, laser irradiation at the same conditions causes damage of the TiPPO layer within 50-60 minutes. This indicates that in the absence of a hydroxyl radical scavenger the photoproducts effectively attack the TiPPO substrate.

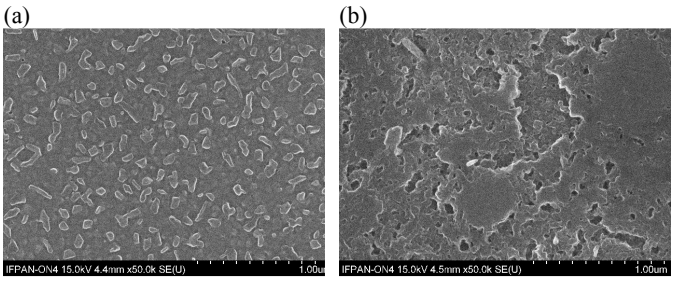

Figure 2. SEM images of a TiPPO layer deposited on a quartz plate: (a) fresh after evaporation, (b) after 4.5 h of irradiation in neat water.

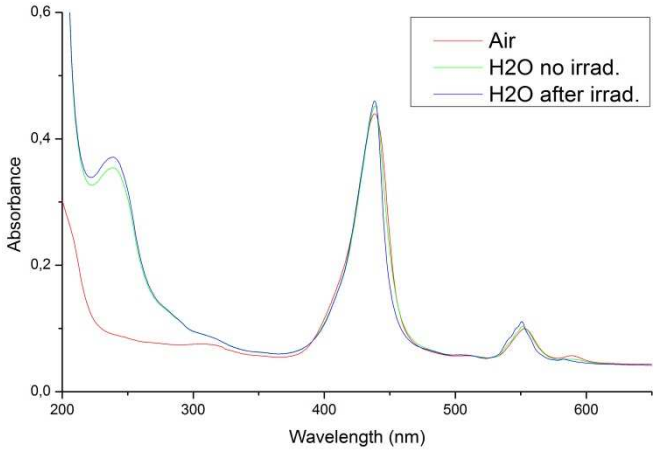

Figure 3. Absorption spectra of TiPPO deposited on a fused silica plate in air (red line), in aqueous TA solution before irradiation (green line), and after 20 minutes irradiation with a 445 nm laser of 50 mW (blue line). The TA and NaOH concentrations are 4.78 x 10^{-4}M and 34.7 x 10^{-4} M, respectively.

Absorption and fluorescence spectra of a TiPPO layer evaporated on a fused silica plate immersed in neat water are shown in Figure 4. The intense Soret band absorbs at 445 nm and the Q-band absorbs with weaker intensity at 555 nm. The absorption spectrum of the TiPPO layer, similar to the absorption spectra of other metallo-tetraphenylporphyrins in the gas phase [23] and TiPPO in solution [24], does not show the vibronic structure of tetraphenylporphyrin seen in thin films [25] and in solution [26]. The positions and relative intensities of the absorption bands of metallo-tetraphenylporphyrins depend on the mixing of metal d orbitals with the π* orbitals on the porphyrin ring [23]. The lack of vibronic structure in the absorbance spectra of TiPPO indicates the existence of such orbital mixing in the TiPPO molecule.

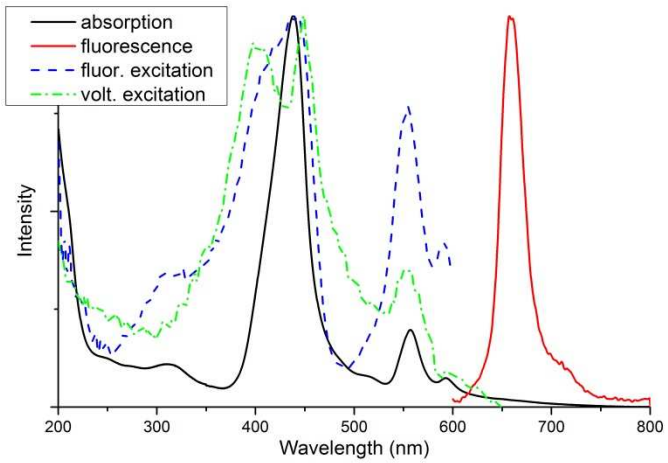

Figure 4. Absorption (black solid line), fluorescence (red solid line) and fluorescence excitation (blue dashed line) spectra of TiPPO on a fused silica plate. The green dot-dashed line represents the dependence of the open circuit voltage on the wavelength of excitation of TiPPO deposited on the gold electrode. The maximum voltage amounts to 0.035 V. The spectra are normalized to equal intensity at the maximum of the Soret band. Absorption and fluorescence spectra were recorded with 1 nm resolution, whereas fluorescence and voltage excitation spectra were recorded with a resolution of 10 nm and 20 nm, respectively. The vertical axis is in arbitrary units.

The vertical excitation energies and oscillator strengths of the lowest singlet states of TiPPO, computed with the TD-DFT method, are collected in Table 1. The relevant frontier molecular orbitals involved in these excitations are the two highest occupied (π_P) and the three lowest unoccupied (π^*_P and d_{Ti}) orbitals of TiPPO. They are essentially the same as for TiOP shown in Fig. 2 of Ref. 15. Analogously to TiPO (Table 1 of Ref. 15), the lowest dipole-allowed excited singlet states involve ππ* excitations within the porphyrin ring of TiPPO (the *Q* band and the *B* band of porphyrin, respectively). The Q_x, Q_y and B_x, B_y states are degenerate in C_{4v} symmetry (^1E). The theoretical results of Table 1 obtained for the isolated TiPPO molecule are in a qualitative agreement with the experimental absorption spectrum of TiPPO evaporated on a fused silica plate (Fig. 4).

Table 1. Vertical excitation energies (ΔE) and oscillator strengths (f) of the lowest excited singlet states of TiPPO computed with the TD-DFT method at the DFT-optimized equilibrium geometry of the ground state.

State	ΔE/eV(λ/nm)	f
$^1\pi_P\pi^*_P$(Q)	2.29(546)	0.11×10^{-2}
$^1\pi_P d_{Ti}$(CT)	2.76(453)	0.0
$^1\pi_P d_{Ti}$(CT)	3.01(415)	0.0
$^1\pi_P\pi^*_P$(B)	3.21(390)	2.13

Like in TiPO, the dipole allowed Q and B states are interloped by two states of CT character, in which a π electron of the porphyrin ring is excited into a *d* orbital of the titanium atom. These states are dark in absorption from the ground state due to the small the overlap of the π_P and d_{Ti} orbitals involved in these transitions (Fig. 2 of Ref. 15).

The shape of the fluorescence spectrum of the system does not depend on the excitation wavelength and its intensity is strong enough to record the fluorescence excitation spectrum of TiPPO in the whole energy range. As shown in Fig. 4, the fluorescence excitation and absorption spectra have qualitatively the same spectral character. Some differences in their shapes may partially result from different spectral resolution (1 nm for absorption versus 10 nm for fluorescence excitation). The intensity of the fluorescence excitation spectrum is corrected using the quantum-counter method. The comparison of the absorption and fluorescence excitation spectra reveals that the S_1 state has a higher fluorescence quantum yield than the S_2 state, as expected due to the photochemically active CT states lying in between them.

To check whether the excitation of TiPPO results in water splitting and production of hydroxyl radicals as proposed for TiPO [15], chemical dosimetry of $OH^{\bullet}$ radicals with TA, as described in the experimental section, was employed. For this purpose, the plates with deposited TiPPO were immersed in an aqueous solution of NaOH and TA and irradiated with visible light. The reaction of TA with $OH^{\bullet}$ radicals converts TA into HTA which is strongly fluorescent when excited at 315 nm. Figure 5a shows a series of HTA fluorescence spectra recorded after 0 to 4.5 hours of irradiation at 445 nm (Soret band absorption) of plates with deposited TiPPO in aqueous TA solution. Before irradiation, the fluorescence spectrum is dominated by the Raman band at 353 nm, which can be assigned to the OH stretching vibration of hydrogen-bonded water. Irradiation of the TiPPO layer results in the buildup of HTA fluorescence centered at 425 nm. The observed increase of the HTA fluorescence intensity vs. irradiation time of the TiPPO layer can be interpreted as evidence of the production of hydroxyl radicals due to the splitting of water.

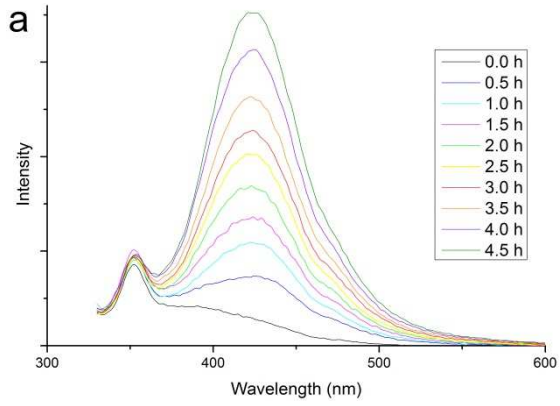

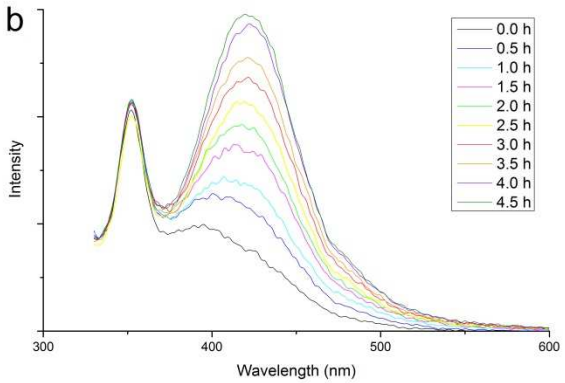

Figure 5. Fluorescence spectra of hydroxyterephthalic acid in water for excitation at 315 nm. Spectra have been recorded after (a) 445 nm and (b) 570 nm irradiation of a TiPPO layer evaporated on a fused silica plate and immersed in a (5 x 10^{-4} M) terephthalic acid/(35 x 10^{-4} M) NaOH solution. The volume of the solution was 3.5 ml. Irradiation was performed in 0.5 hour increments, with breaks for HTA fluorescence measurements. The legend specifies the total irradiation time for each spectrum.

To find out how the process of hydroxyl radical generation depends on the wavelength of excitation, we irradiated a TiPPO-deposited plate with light at 570 nm (Q-band). The results are shown in Fig. 5b. The HTA fluorescence spectra presented in Figs. 5a and 5b were taken under identical conditions, but the wavelength and power of the irradiating light were different and the absorbance at those wavelengths was different as well. To correct the intensity of HTA fluorescence for those differences, we divided the measured integral intensity by a factor proportional to absorbed irradiation flux. These integrated intensities are presented in Fig. 6 as functions of the time of irradiation. Both sets of experimental points show a linear dependence on time and no saturation is observed for up to 4.5 hours. The HTA fluorescence increases faster when TiPPO is excited at 445 nm (Soret band) than at 570 nm (Q-band). The linear fit to the data reveals that the slope for the 445 nm excitation is 1.74 times higher than the slope for the 570 nm excitation. This indicates that the yield of hydroxyl radicals is higher for the excitation of the Soret band than the Q-band.

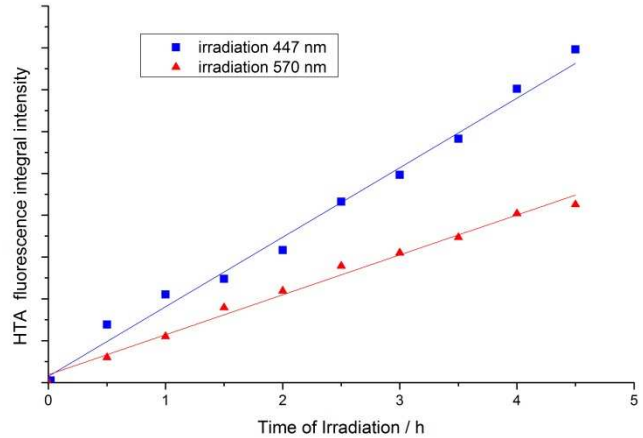

Figure 6. Dependence of the integrated intensity of the HTA fluorescence spectrum presented in Fig. 2 on the duration of irradiation. The intensities were corrected for the number of absorbed photons by taking into account the differences in the wavelength, power of irradiating light and in absorbance of the TiPPO layer at each wavelength.

To check whether photoinduced water oxidation occurs in pure water (without NaOH), experiments with BA as $OH^{\bullet}$ scavenger were performed. The lowest excited singlet state of BA absorbs at 271 nm in aqueous solution and exhibits a fluorescence spectrum with a maximum at 312 nm (Fig.7). Excitation of the solution at 300 nm results in the strong Raman line of water (at 333 nm) and weak fluorescence at longer wavelengths, probably of BA aggregates which are likely to occur at this relatively high concentration.

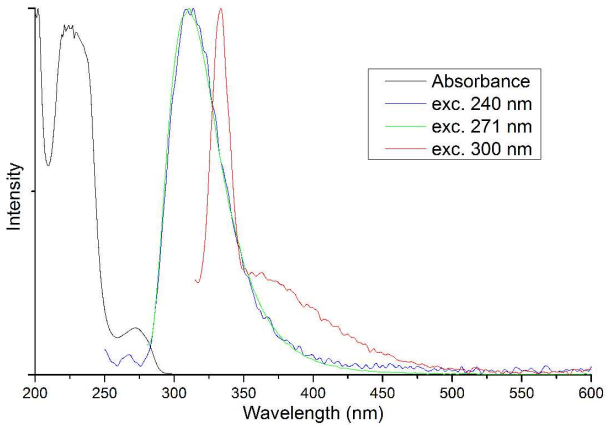

Figure 7. Normalized absorbance (black line) and normalized fluorescence spectrum of benzoic acid in neat water at different excitations: 240 nm (blue line), 271 nm (green line) and 300 nm (red line). The concentration of benzoic acid is 4.22 x 10^{-4} M.

Photo-irradiation of a TiPPO layer immersed in an aqueous solution of BA results in the build-up of salicylic acid fluorescence (Fig. 8). The SA fluorescence spectrum has a maximum at 405 nm and is of relatively weak intensity, as reported earlier [28]. The large Stokes shift of the SA fluorescence may originate from the excited-state intramolecular proton transfer (ESIPT) process in SA [29].

The integrated intensity of SA fluorescence increases linearly with the time of photo-irradiation (inset of Fig. 8), similar to the HTA case. The growth of the SA fluorescence proves that BA to SA conversion occurs in the solution. It provides an indirect proof of the generation of hydroxyl radicals upon photo-irradiation of TiPPO.

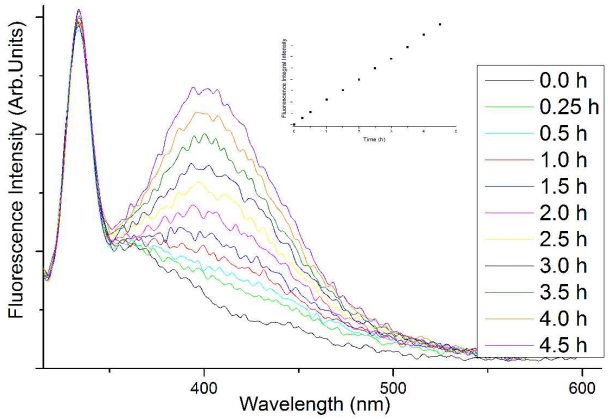

Figure 8. The build-up of salicylic acid fluorescence due to photo-irradiation of a TiPPO layer at 445 nm with a power of 45 mW. The plate with deposited TiPPO was immersed in 3 ml solution of neat water with 4.22 x 10^{-4} M benzoic acid. The spectra were recorded with excitation at 300 nm. The legend specifies the total time of photo-irradiation. The inset presents the integral intensity of SA fluorescence versus the time of photo-irradiation.

Efficiency of water splitting via the radical channel

Figs. 5 and 6 show that in a volume of 3.5 ml of the solvent the fluorescence of HTA grows linearly with time for several hours. To observe the saturation of the fluorescence intensity (due to the consumption of TA by conversion to HTA), we used small cuvette containing 0.2 ml of H_2O with 3.54 x 10^{-3} M NaOH and 4.78 x 10^{-4} M TA. In this case, we were able to reach saturation of the HTA fluorescence within about ten minutes of irradiation (Fig. 9). The characteristic time of the HTA fluorescence build-up, determined by a fit of the HTA fluorescence evolution with exponential functions, ranges from 3 to 11 minutes, depending on the laser power.

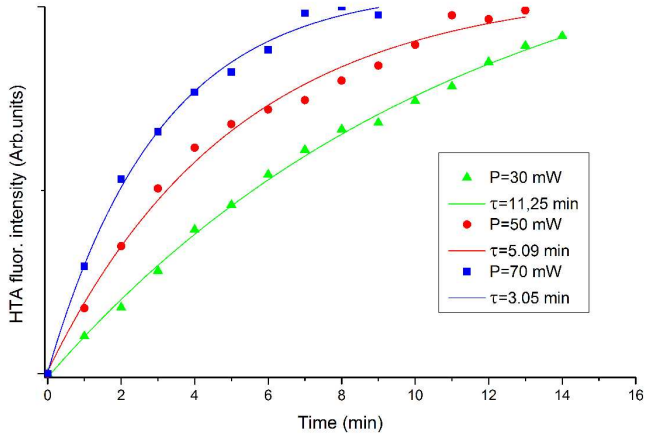

Figure 9. Increase of the integral HTA fluorescence intensity resulting from the irradiation of a TiPPO layer (area 1.2 cm^2) with a 445 nm laser. The fused silica plate with the TiPPO layer was immersed in 0.2 ml of H_2O with 35.38 x 10^{-4} M NaOH and 4.78 x 10^{-4} M TA. Laser power and build-up times are specified in the legend. The solid curves represent a fit of the expression $A(1-e^{-t/\tau})$ to the experimental data, where τ is the build-up time and A is the initial TA concentration.

The rate constant for the HTA build-up (reciprocal of the characteristic time τ) grows linearly with the laser power (Fig. 10). This excludes that H_2O_2 (formed by $OH^{\bullet} + OH^{\bullet} \rightarrow H_2O_2$ recombination) contributes to the consumption of TA molecules. Since the absorption spectrum of the TiPPO Soret band is essentially the same before and after irradiation (Fig. 3), destruction of the molecular layer is negligible. We thus conclude that reaction (2) is the main path for the disappearance of TA and the saturation of the HTA fluorescence intensity. From the laser intensity, the optical density of the TiPPO layer and the initial concentration of TA, one can calculate the rate constants and efficiencies for the chain reactions (1) and (2). The results are presented in Table 2. The yield of $OH^{\bullet}$ radicals is at least 2 times higher than the yield of HTA, since two $OH^{\bullet}$ radicals are required to convert TA into HTA (reaction 2).

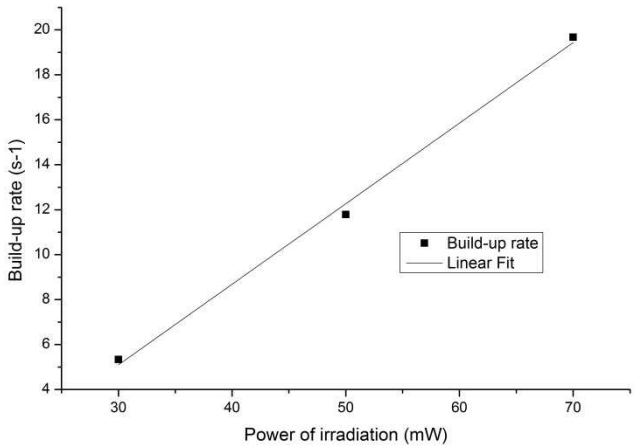

Figure 10. Rate constant of HTA fluorescence build-up vs. irradiating laser power. The experimental conditions described in Fig. 9.

Table 2. Quantum efficiency and rate constant for the build-up of HTA concentration, representing ½ of the lower-limit for hydroxyl radical generation (see reaction 2). Efficiency is defined as the number of HTA molecules generated per absorbed photon.

Initial TA concentration [M]	Laser power [mW]	Efficiency	HTA build-up rate [M/s]
4.78×10^{-4}	30	3.07×10^{-3}	7.08×10^{-7}
4.78×10^{-4}	50	4.11×10^{-3}	1.56×10^{-6}
4.70×10^{-4}	50	4.33×10^{-3}	1.66×10^{-6}
4.78×10^{-4}	70	5.32×10^{-3}	2.60×10^{-6}

The values of the efficiency and the rate constant increase with laser power. This may reflect the competition between different reactions by which $OH^{\bullet}$ radicals recombine [17] and the dependence of these reactions on the concentration of hydroxyl radicals. Let us note that the estimated rate of HTA generation in our experiment, 10^{-6} M/s (an indirect lower-limit estimation of $OH^{\bullet}$ radical generation), is three orders of magnitude higher than the rate of 10^{-9} M/s reported for HTA generation by a pulsed discharge on a water surface [17].

Efficiency of water splitting via the ionic channel

We have tried to check whether the generation of other, especially electrically charged, products is possible in the reaction. For this purpose, measurements of voltage and electric current were performed for TiPPO deposited on a gold electrode and immersed in distilled and deionized water. Using gold electrodes and neutral (no electrolyte) aqueous solution, we have eliminated factors that could have provided a bias for the radicalic water splitting process versus the generation of charged products. Under such "clean" conditions we have detected a weak response to irradiation: a photocurrent of very low intensity and a photoinduced voltage. The values of the short circuit current intensity and open circuit voltage are presented in Table 3. The photon to electric charge conversion quantum efficiency is extremely low, of the order of 10^{-6}, and decreases at longer wavelengths of excitation. The open-circuit voltage excitation spectrum (not shown) is generally similar to the absorption and fluorescence excitation spectra, except for excitation within the Soret band, where a peak splitting of 2900 cm^{-1} is clearly seen, in contrast to the absorption spectrum. This may indicate that the weak voltage excitation spectrum originates from surface states which are masked in the absorption spectrum by the bulk of the absorber.

Table 3. Photovoltaic data obtained for TiPPO in deionized water. The illuminated area is 1.2 cm^2. V_{oc} – open circuit voltage, I_{sc} – short circuit current intensity, Efficiency equals to the number of generated elementary charges per absorbed photon.

Wavelength [nm]	V_{oc} [V]	I_{sc} [μA]	Efficiency
445	0.26	0.1	4.6×10^{-6}
570	0.24	0.11	2.4×10^{-6}

Discussion

The theoretical results of Ref. 15 indicate that the dark CT states of the TiPO-H_2O hydrogen-bonded complex provide a mechanism for the splitting of the water molecule to yield the $TiPOH^{\bullet}$ - $OH^{\bullet}$ radical pair. Like in TiPO, in TiPPO the reactive CT states are theoretically predicted in between the absorbing Q and B bands. The present experimental results show that splitting of water occurs upon excitation of TiPPO within both absorption bands. This means that the reactive state for water splitting can be populated from both absorbing excited electronic states.

In Fig. 9, the potential-energy diagram relevant for the photo-catalyzed water splitting reaction in the TiPPO-H_2O hydrogen-bonded complex is displayed. The left hand side shows the vertical excitation energies of the lowest excited singlet states (blue and red dashed lines) computed with the TD-DFT method at the DFT-optimized ground-state geometry of the complex. On the right hand side, the DFT energy of the radical pair computed at its equilibrium geometry is shown (solid red line).

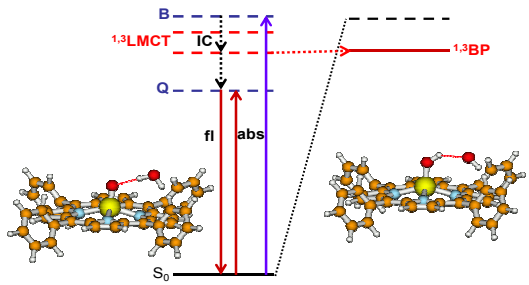

Figure 9. Potential-energy diagram illustrating the photo-catalyzed water splitting reaction in the TiPPO-H_2O complex. The vertical excitation energies of the lowest excited singlet states of the complex are given by the dashed lines on the left hand side. The solid red line on the right hand side represents the energy of the $TiPPOH^{\bullet}$-$OH^{\bullet}$ biradical pair, while the dashed black line denotes the energy of the $TiPPOH^{+}$-OH^{-} ion pair at this geometry.

Fig. 9 indicates that the formation of the radical pair is energetically feasible for optical excitation within the Soret band and that the reaction is thermoneutral from the lowest CT state. On the other hand, the reaction is predicted to be endoenergetic for excitation of the Q band. One has to keep in mind, however, the approximate nature of the computational results. This concerns, in particular, the

comparison of the TD-DFT excited-state energy of the TiPPO-H_2O complex (which is generally underestimated) with the UDFT energy of the biradical (which is usually overestimated). Moreover, the computational results were obtained for the isolated TiPPO-H_2O complex, while the experimental measurements were performed for molecular micro-crystals immersed in an aqueous environment. Fig. 9 thus provides only a qualitative explanation of the mechanism of the photocatalytic oxidation of water by visible light. Additionally, we cannot exclude that the reaction from the Q band is thermally promoted due to a locally elevated temperature at the irradiated TiOPP surface. The effects of surface melting can in fact be noticed upon inspection of the SEM images shown in Fig. 2.

Conclusions

Photocatalytic splitting of water was investigated in a heterogeneous system consisting of micro-crystallites of TiPPO deposited on a silica plate, immersed in water and excited via the Q and B bands of the metalloporphyrin.. The experimental results seem to confirm the mechanism of water splitting and generation of $OH^{\bullet}$ radicals proposed theoretically by Sobolewski and Domcke [15] for the TiPO-H_2O complex. The observation of a small photocurrent reveals another, albeit very inefficient, ionic mechanism of water splitting. In both cases, the oxidation of water occurs without pH-bias (electrolyte is not required) and without an external potential bias. Moreover, the rate of THA generation is by orders of magnitude higher than in other known to us experiment.

Acknowledgments

We thank the NCN (National Science Center of Poland) for funding this project; grant no. 2012/04/A/ST2/00100. This work was partially supported by the European Union within the European Regional Development Fund through the Innovative Economy grant MIME (POIG.01.01.02-00-108/09). We thank Professor W. Domcke for stimulating discussions in the course of the study.

Notes and references

Institute of Physics Polish Academy of Sciences, Al. Lotników 32/46, 02-668 Warsaw, Poland
* Corresponding author. E-mail: sobola@ifpan.edu.pl
Electronic Supplementary Information (ESI) available: [details of any supplementary information available should be included here]. See DOI: 10.1039/b000000x/

1 A. Fujishima and K. Honda, *Nature*, 1972, **238**, 37.
2 T. Bak, J. Nowotny, M. Rekas and C. C. Sorrell, *Int. J. Hydrogen Energy*, 2002, **27**, 991.
3 A. J. Esswein and D. G. Nocera, *Chem. Rev.*, 2007, **107**, 4022.
4 R. M. N. Yerga, M. C. A. Galvan, F. del Valle, J. A. V. de la Mano and J. L. G. Fierro, *ChemSusChem*, 2009, **2**, 471.
5 K. Maeda and K. Domen, *J. Phys. Chem. Lett.*, 2010, **1**, 2655.
6 M. G. Walter, E. L. Warren, J. R. McKone, S. W. Boettcher, Q. Mi, E. A. Santori and N. S. Lewis, *Chem. Rev.*, 2010, **110**, 6446.
7 X. Chen, S. Shen, L. Guo and S. S. Mao, *Chem. Rev.*, 2010, **110**, 6503.
8 M. R. Wasielewski, *Chem. Rev.*, 1992, **92**, 435.
9 D. Gust, T. A. Moore and A. L. Moore, *Acc. Chem. Res.*, 2001, **34**, 40.
10 J. H. Alstrum-Acevedo, M. K. Brennaman and T. J. Meyer, *Inorg. Chem.*, 2005, **44**, 6802.
11 H. Imahori, Bull. *Chem. Soc. Jpn.*, 2007, **80**, 621.
12 V. Balzani, A. Credi and M. Venturi, *ChemSusChem*, 2008, **1**, 26.
13 S. Fukuzumi, *Phys. Chem. Chem. Phys.*, 2008, **10**, 2283.
14 D. Gust, T. A. Moore and A. L. Moore, *Faraday Discuss.*, 2012, **155**, 9.
15 A. L. Sobolewski, W. Domcke, Phys. Chem. Chem. Phys., 2012, **14,** 12807.
16 P. Fournari, R. Guilard, M. Fontesse, J.-M. Latour and J.-C. Marchon, *Journal of Organometallic Chemistry* 1976, **110**, 205
17 S. Kanazawa et al., *Plasma Sources Sci. Technol*, 2011 **20,** 034010.
18 K. Ishibashi, A. Fujishima, T. Watanabe et al., *Electrochemistry Communications*, 2000, **2**, 207.
19 Q. Xiao et al., *J. of Hazardous Materials*, 2008, **150**, 62.
20 D. E. Woon and T. H. Dunning, Jr., *J. Chem. Phys.*, 1993, **98**, 1358.
21 R. Ahlrichs, M. Bär, M. Häser, H. Horn and C. Kölmel, Chem. Phys. Lett., 1989, **162**, 165.
22 C. Hättig, Adv. Quantum. Chem., 2005, **50**, 37.
23 L. Edwards and D. H. Dolphin, *J. Mol. Spectrosc.*, 1971, **38**, 16.
24 M. Hoshino, M. Imamura, S. Watanabe, Y. Hama, *J. Phys. Chem.*, 1984, **88**, 45.
25 M. M. El-Nahass et al., *Spectrochimica Acta Part A*, 2005, **61**, 3026.
26 D. F. Marsh, L. M. Mink, *J. Chem. Education*, 2005, **73**, 1188
27 G. W. Klein, K. Bhatla, V. Madhavan, and R. H. Schuler, *J. Phys. Chem.*, 1975, **79**, 1767. –
28 M. M. Karim, H. S. Lee, Y. S. Kimb, H. S. Baeb, S. H. Lee, *Analytica Chimica Acta,* 2006, **576**, 136.
29 P. B. Bisht, H. Petek, K. Yoshihara, *J. Chem. Phys*. 1995, 103 5290.
30 D. Vulpius, G. Geipel, G. Bernhard, *Spectrochimica Acta Part A*, 2010, **75**, 558.

TOC graphic

TiOPP very efficiently catalyses photooxidation of water with visible light.